Rev. Roum. Sci. Techn.– Électrotechn. et Énerg.
Vol. **66**, *3*, pp. 153–160, Bucarest, 2021

IMPROVED DECOUPLING VIRTUAL SYNCHRONOUS GENERATOR CONTROL STRATEGY

YACINE DAILI[1], ABDELGHANI HARRAG[1]

Key words: Virtual synchronous generator, Vector synchronous generator (VSG), Microgrid, Renewable energy sources, Distributed generator, Grid stability.

The virtual synchronous generator (VSG) concept is one of the promising solutions to facilitate the integration of the renewable DG into microgrid. It consists in controlling the inverter-based DG to mimic synchronous machine characteristics leading to the grid stability improvement in case of high penetration level of renewable energy into the microgrid. The line impedance in low voltage and medium microgrids is present resistive or mixed resistive-inductive property. Therefore, the active and reactive powers are nonlinear functions and strongly coupled, which result in poor dynamic performance even instability of the DG based on conventional VSG control. To eliminate such coupling and enhance the stability and dynamic performance, a new decoupled VSG is proposed based on the injection of two additional control signals to the control variables in transit steady state, the expression of the control signals is obtained by applying a small signal approach. The proposed VSG control has been implemented and compared to conventional one using Matlab/Simulink. Simulation results show a significant improvement in the overshoot and setting time reduction 66.60 % and 99.55 %, respectively. Additionally, robustness results realized using a line parameters variation confirm the effectiveness of the proposed VSG control.

1. INTRODUCTION

During last decades, distributed generation (DG) systems based on renewable energy sources, such as wind turbines, fuel cell and photovoltaic have been proposed for overcoming the challenges of integrating renewable energy sources into the existing micro-grid. Dc/ac power electronics converter has been widely used to interface the DGs based renewable energy sources and energy storage system [1]. The penetration of power electronic converter into the existing utility grid has been increased as the same time of the renewable energy, Consequently, the rotating inertia of the power system is reduced, which could cause a stability problem. In recent years, many researchers have focused their research toward the development of the inverter-based DG control strategies to facilitate the integration of the renewable energy to the main grid [2,4].

Traditionally, the control technique of the inverter-based DG units are operated in current controlled mode, a phased-locked-loop (PLL) is used to synchronous the inverter to the utility grid, the inverter current is controlled to injected predefined active and reactive powers into the grid [5]. However, this control technique has not the ability to operate in islanding mode. Moreover, by applying such a control strategy, the inverter cannot provide any inertia to the power system. Consequently, the disturbances or sudden changes in generation or loads can cause a stability degradation of the power system with a high-level penetration of the renewable energy [6, 3].

The droop control scheme and virtual synchronous generator (VSG) control method are widely employed in DG units due to their independent and wireless control [7–10]. These control techniques can ensure both grids connected and island modes operating of DG units. The droop control scheme was originally proposed in [11,12] for parallel uninterruptible power supply (UPS) systems. The injected active and reactive power regulation is achieved by imitating static operation characteristics of synchronous generators (SGs). However, droop control scheme has no inertia support for the power system [13]. Virtual synchronous generator known also as synchronverters [10], it is an emerging novel concept to handle stability issues of micro-grid with inverter-based DG. This technique was introduced by [14]. The basic idea of the VSG is to control in real time the DG inverter to mimic the dynamic behaviour of synchronous generators, the inertia characteristic emulated by the VSG contributes to the total inertia of the grid. Consequently, the inverter based DGs can directly participate in providing the required frequency and voltage support for the microgrid. On the other side, the VSG control technique and droop control strategy have the same dynamic if an appropriate filter is incorporated into a conventional droop control scheme [3].

DG units are commonly connected to the microgrid through medium and low voltage line, where the line impedance is not purely inductive, or the power angle is not enough small. As result, a strong coupling between active and reactive power is occurred when conventional control methods are applying, such coupling could impact the stability and dynamic performance of the power system [15–18].

In the literature, several improved VSG and droop control methods have been presented to addresses the aforementioned challenges, which can be classified into three categories:

- Virtual impedance method have been used to reduce the influence of power coupling, it consists on adding an appropriate virtual impedance to make the total line impedance propriety mainly inductive. However, the virtual impedance value is limited by the bus voltage droop and stability of the micro-grid [19–22]. Improved power decoupling can be obtained using a negative resistance to contract the line resistance. Nevertheless, the system could become instable if the line resistance drafts, which limits its practical applications [22].
- Virtual frame transformation method is another way to decouple between active and reactive power in presence of a mixed line impedance, the decoupling is realised through introducing orthogonal rotational matrix from active reactive power to the modified active and reactive

[1] Mechatronics Laboratory (LMETR), Optics and Precision Mechanics Institute, Ferhat Abbas University of Sétif, 19000 Setif, Algeria

power, the matrix transformation is expressed in term of the line impedance angle [23,24]. Although this method can guarantee effective decoupling between active and reactive power and improve the stability and transient performance of the system, it cannot achieve complete decoupling due to its sensitivity to the line impedance angle value [16,25]. Moreover, for multiple DG units with different line impedance angle, the reference frame well be not the same and the references frame of the DG units well be out the synchronism [26].

- Compensation based method was proposed in [27, 28], it consists on injecting additional control signals to reduce the influence of power coupling in micro-grids. In [27] the decoupling is realised by means of tow auxiliary control signals; these signals are calculated based on an online parameter identification algorithm. The main problem of this approach is that the dynamic performance depends on speed adaptation of the parameter identification algorithm. Ref. [28] has improved the method reported in [27] by employing a gain scheduled scheme. However, both of this technique cannot be applied to the grid-connected mode [29].

In this paper, a novel technique for VSG control has been proposed in order to eliminate the mutual influence between active and reactive power. Thus, the dynamic and stability of the active and reactive power loops well be enhanced based on the injection of new control signals in the active and reactive power loops in transit steady state to reduce the effect of power coupling.

The decoupling signals are synthesized based on linear model of system obtained by applying à small signal method. Simulation results show a considerable improvement in the reduction of the overshoot and setting time.

In addition, robustness results realized using a line parameters variation confirm the effectiveness of the proposed VSG decoupling control. The coupling effect between active and reactive power is almost eliminated without influencing the inertia support feature of VSG control. Therefore, the oscillations and overshoots of active and reactive power are reduced and the system recover the steady state rapidly. The rest of the paper is organized as follows: Section 2 presents the material and methods including principle of virtual synchronous generator principle, the small signal modelling of the VSG as well as the proposed VSG control scheme. Section 3 presents the simulations results and discussions. While Section 4 stated the main conclusions of this work.

2. MATERIAL AND METHODS

2.1 CONVENTIONAL VSG CONTROL STRATEGY

Fig. 1 illustrated the DG topology using the traditional VSG control technique.

From Fig. 1, we assume:

- To simplify the studies, the DC source is used instead of distributed generation (DG);
- The three-phase voltage source inverter (VSI) is connected to the main grid at the point of common coupling (PCC) through an LC filter where L_F and C_F are filter inductance capacitor, respectively;
- Z_L is the line impedance including the resistance and inductance denoted R_L and L_L, respectively.
- v_m and v_g are the instantaneous voltage of the inverter and the grid, respectively;
- v_m and v_g are the instantaneous voltage of the inverter and the grid, respectively;
- δ is the electrical angle, which is the difference between VSG voltage phase θ_m and grid voltage phase θ_g.

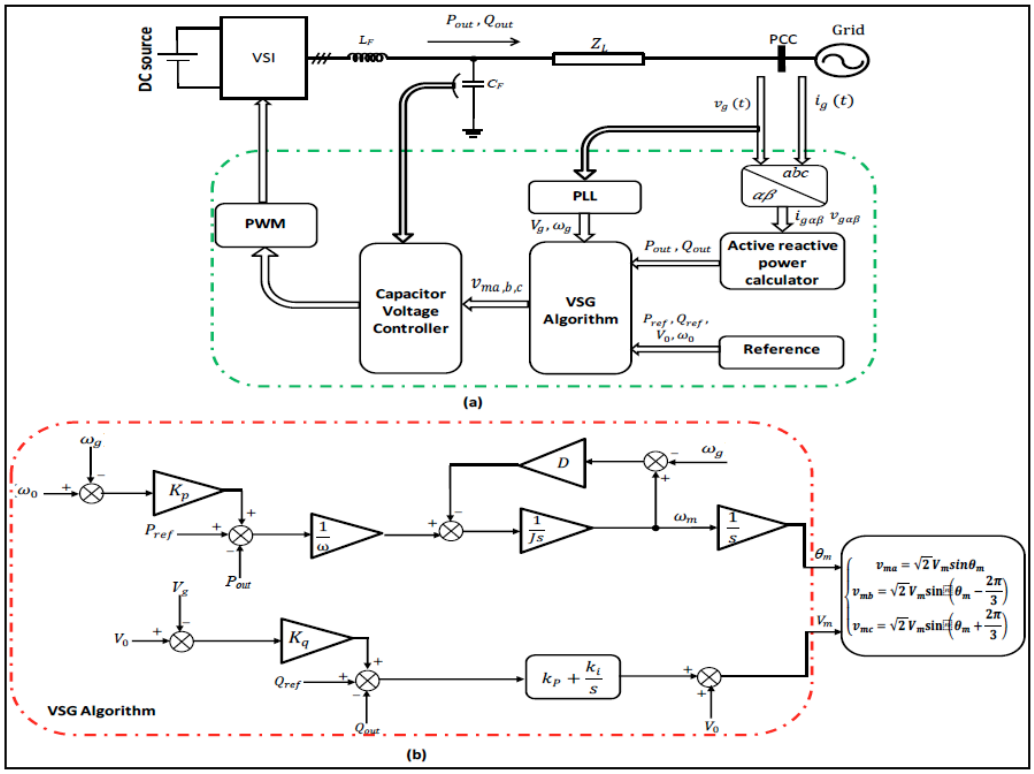

Fig. 1 – Topology and control structure of VSG.

The active power P_{out} and reactive power Q_{out} injected in the grid are computed from v_g and i_g in αβ reference frame:

$$\begin{cases} P_{out} = V_{g\alpha} I_{g\alpha} + V_{g\beta} I_{g\beta}, \\ Q_{out} = V_{g\beta} I_{g\alpha} - V_{g\alpha} I_{g\beta}. \end{cases} \quad (1)$$

Based on VSG control principle, the active power controller of the VSI implements in real time the mechanical dynamic model of the synchronous generator (SG) using the following expression [30]:

$$\begin{cases} \dfrac{P_{in} - P_{out}}{\omega_g} = D(\omega_g - \omega_m) + J\dfrac{\mathrm{d}\omega_m}{\mathrm{d}t}, \\ \dfrac{\mathrm{d}\theta_m}{\mathrm{d}t} = \omega_m; \dfrac{\mathrm{d}\theta_g}{\mathrm{d}t} = \omega_g, \end{cases} \quad (2)$$

where J is the rotational inertia, D is the damping coefficient, P_{in} is the input power, P_{out} is the electrical output power, ω_g is the grid angular velocity and ω_m is the virtual rotor angular velocity.

The grid angular velocity ω_g is detected at the PCC by the phased looked loop PLL system, then the virtual rotor speed ω_m is calculated by solving the mechanical equation (eq. 2). The virtual mechanical phase angle θ_m is produced by the integration of ω_m. To accomplish the active power regulation, the input power P_{in} is generated by an outer frequency droop regulator according to equation (eq. 3), which simulates the governor of the conventional SG [31].

$$P_{in} = P_{ref} + K_p(\omega_0 - \omega_g), \quad (3)$$

where P_{ref} is the active power reference value, ω_0 is the rated angular velocity, K_p is the active droop coefficient.

Similarly, the reactive power control loop emulated the conventional excitation circuit of a real SG. The control loop includes a reactive power droop mechanism equation (eq. 4) and a voltage regulator equation (eq. 5) [32]:

$$Q_{in} = Q_{ref} + K_q(V_0 - V_g), \quad (4)$$

$$V_m = \left(K_p + \frac{K_i}{s}\right)(Q_{in} - Q_{out}) + V_0, \quad (5)$$

where V_g is the root-mean-square (RMS) value of the grid voltages, V_0 is the no-load voltage, K_q is the reactive droop coefficient, k_i and k_p are the integral and proportional coefficients of the voltage regulator and Q_{ref} is the reference value of reactive power.

The active and reactive droop coefficient K_p and K_q are fixed by the local grid standard [16, 33]. In this study, we use a change of 100 % in active power corresponding to a variation of 1 % of the grid frequency and a change of 100 % in reactive power corresponding to a variation of 5 % of the grid nominal voltage.

Finally, the amplitude voltage V_m and the virtual mechanical phase angle θ_m are used for synthesizing the references voltages (v_{ma}, v_{mb}, v_{mc}), which are the inputs of voltages controllers. The voltage references can be written:

$$\begin{cases} V_{ma} = \sqrt{2} V_m \sin(\theta_m) \\ V_{mb} = \sqrt{2} V_m \sin(\theta_m - \dfrac{2\pi}{3}), \\ V_{mc} = \sqrt{2} V_m \sin(\theta_m + \dfrac{2\pi}{3}) \end{cases} \quad (6)$$

The voltage controllers is introduced to track accurately the voltage references. The outputs of the voltage controller are fed into the PWM modulator to the drive the inverter signals.

2.2 SMALL SIGNAL SYSTEM MODELLING

Considering the equivalent model of microgrid where two nodes have line to line voltage V_m and V_g are interconnected by a line impedance Z_L. The output active and reactive power injected in the grid could be expressed by [34]:

$$P_{out} = \frac{R_L V_m^2 - R_L V_m V_g \cos(\delta) + X_L V_m V_g \sin(\delta)}{R_L^2 + X_L^2}, \quad (7)$$

$$Q_{out} = \frac{X_L V_m^2 - X_L V_m V_g \cos(\delta) - R_L V_m V_g \sin(\delta)}{R_L^2 + X_L^2}, \quad (8)$$

where δ is the load angle given by:

$$\delta = \theta_g - \theta_m = \int (\omega_g - \omega_m)\mathrm{d}t. \quad (9)$$

Normally, for a large synchronous generator coupled to the grid through a high voltage line, the line impedance is manly inductive, and the load angle is enough small; thus the expressions of the active and reactive powers equations eqs. (7) and (8) become:

$$P_{out} = \frac{V_m V_g}{X_L}\delta, \quad (10)$$

$$Q_{out} = \frac{V_m}{X_L}(V_m - V_g). \quad (11)$$

Therefore, the active power is controlled by the angle δ and the reactive power is regulated by changing in the inverter output voltage V_m amplitude (see Fig. 1). However, the above assumption is not correct for a low or medium voltage line where the line impedance in these cases is not dominantly inductive which makes active and reactive powers as nonlinear functions. Additionally, they are not independent, changes of V_m and δ affect both P_{out} and Q_{out} variations. This behaviour makes the control of active and reactive powers more complicated.

In order to find out a linear relationship between control variables (δ and V_m) and output power of DG system (P_{out} and Q_{out}), a small signal method is explored [35]. By linearizing equations eqs. (7) and (8) around an equilibrium point denoted by superscript "0", the small perturbations of the active and reactive powers denoted by ΔP_{out}, ΔQ_{out} resulting from small variations of the input variables $\Delta\delta$ and ΔV_m, given by the following equations:

$$\Delta P_{out} = K_{P-V_m}\Delta V_m + K_{P-\delta}\Delta\delta, \quad (12)$$

$$\Delta Q_{out} = K_{Q-V_m}\Delta V_m + K_{Q-\delta}\Delta\delta, \quad (13)$$

where:

$$K_{P-V_m} = \frac{P_0}{V_{t0}} + \frac{R_L V_{m0}}{R_L^2 + X_L^2}, \quad (14)$$

$$K_{P-\delta} = -Q_0 + \frac{X_L V_{m0}^2}{R_L^2 + X_L^2}, \quad (15)$$

$$K_{Q-V_m} = \frac{Q_0}{V_{t0}} + \frac{X_L V_{m0}}{R_L^2 + X_L^2}, \quad (16)$$

$$K_{Q-\delta} = P_0 - \frac{R_L V_{m0}^2}{R_L^2 + X_L^2}. \quad (17)$$

P_0, Q_0 and V_{m0} are the active power, the reactive power and the inverter voltage at the equilibrium point, respectively. Likewise, the deviations of the active and reactive controllers' equations (eqs. 2 to 5) become:

$$\Delta P_{in} - \Delta P_{out} = D\omega_{g0}\left(\Delta\omega_g - \Delta\omega_m\right) + J\omega_{g0}s\Delta\omega_m, \quad (18)$$

$$\Delta P_{in} = \Delta P_{ref} - K_p\Delta\omega_g, \quad (19)$$

$$\Delta Q_{in} = \Delta Q_{ref} - K_q\Delta V_g, \quad (20)$$

$$\Delta V_m = \left(K_g + \frac{K_i}{s}\right) + (\Delta Q_{in} - \Delta Q_{out}). \quad (21)$$

From equations eqs. (12) to (21), the linear model of active and reactive powers loops of Fig. 1 can be derived as illustrated in Fig. 2.

The inner voltages loop is considered as a follower in the forward path of the power loop. The model inputs are the micro-grid frequency and voltage amplitude deviations.

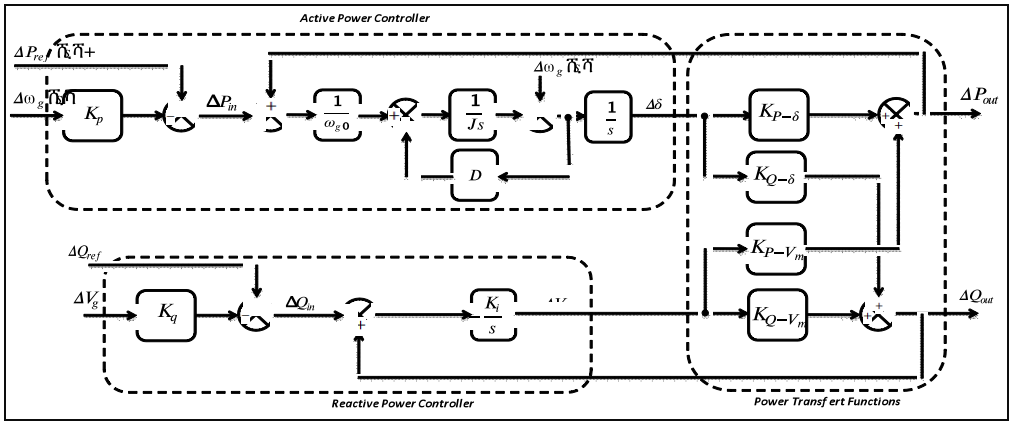

Fig. 2 – Small signal model of the active and reactive powers loops.

While the outputs of the system are the active and reactive powers deviations injected by the DG system. The microgrid frequency and voltage amplitude deviations could be a result of a transit of the micro-grid load or a connection- disconnection of other DG systems.

2.3 PROPOSED DECOUPLING VSG CONTROL SCHEME

From Fig. 2, it is worth noting that the variation of the reference active power/PCC frequency affect both voltage and velocity of the inverter. In the same way, the variation of the reactive power/PCC amplitude voltage affect both V_m and δ. The active and reactive powers coupling could cause the system stability problem. To enhanced transient performance and stability of the system, the coupling between active and reactive power loop should be reduced as much as possible.

Based on equations eqs. (12) and (13), if the terms $K_{P-V_m}\cdot\Delta V_m$ and $K_{Q-\delta}\cdot\Delta\delta$ in active and reactive power expressions are forced to zero, the active and reactive power deviation dynamics can be decoupled becoming depending separately on voltage and load angle, respectively. To this aim, two additional control signals $\lambda\Delta\delta'$ and $\beta\Delta V_t^{'}$ have been introduced as follows:

$$\Delta V_t = \Delta V_t^{'} + \lambda\Delta\delta', \quad (22)$$

$$\Delta\delta = \Delta\delta' + \beta\Delta V_t^{'}. \quad (23)$$

By substituting equations eqs. (22) and (23) in equations eqs. (12) and (13), we have:

$$\Delta P = K_{P-Vt}\left(\Delta V_t^{'} + \lambda\Delta\delta'\right) + K_{P-\delta}\left(\Delta\delta' + \beta\Delta V_t^{'}\right), \quad (24)$$

$$\Delta Q = K_{Q-Vt}\left(\Delta V_t^{'} + \lambda\Delta\delta'\right) + K_{Q-\delta}\left(\Delta\delta' + \beta\Delta V_t^{'}\right). \quad (25)$$

Setting the active and reactive power deviation as:

$$\Delta P = A\Delta\delta' \quad (26)$$

$$\Delta P = B\Delta\delta' \quad (27)$$

Comparing equations eqs (26) and (27) to equations eqs. (24) and (25), A and B can be defined by:

$$A = \frac{K_{P-\delta}K_{Q-\delta} - K_{P-Vt}K_{Q-Vt}}{K_{Q-\delta}}, \quad (28)$$

$$B = \frac{K_{Q-Vt}K_{P-\delta} - K_{Q-\delta}K_{P-Vt}}{K_{P-\delta}}, \quad (29)$$

Solving for λ and β, we obtain:

$$\lambda = -\frac{K_{Q-Vt}}{K_{P-\delta}} = \frac{\frac{Q_0}{V_{t0}}\left(R_L^2 + X_L^2\right) + X_L V_{t0}}{-P_0\left(R_L^2 + X_L^2\right) + R_L V_{t0}^2}, \quad (30)$$

$$\beta = -\frac{K_{P-Vt}}{K_{P-\delta}} = \frac{\frac{P_0}{V_{t0}}\left(R_L^2 + X_L^2\right) + R_L V_{t0}}{Q_0\left(R_L^2 + X_L^2\right) - X_L V_{t0}^2}. \quad (31)$$

Here the issue now is the identification of the coefficients λ and β to compute the decoupling control signals $\lambda\Delta\delta'$ and $\beta\Delta V_t'$. It is noted that these coefficients are expressed in terms of line impedance parameters (R_L and X_L) and the steady-state values of P_0, Q_0 and V_{t0}.

These steady-state values λ and β could be estimated by an online recursive least square identification algorithm [27]. However, using such estimator increase the complexity of the control system. Moreover, the performance of the controller depends on properties of the speed of adaptation of identification algorithm. The steady state values for a given operating point are calculated by small signals quantities from instantaneous signals. The small signal components, which represent fast transition quantities of (ΔP, ΔQ and ΔV_t), are obtained by passing the corresponding signals through a high pass filter [28]. Nevertheless, the use of high filter introduces a phase error which render the decoupling processes ineffective. In this paper, the synthesis of the decoupling control signals have been performed as follows:

- **Detection of the transient steady state:** in this step the active or reactive power is sampling and compared for two successive sampling instants; if the difference exceeds certain threshold this means that a dynamic steady state is observed. In this case, a flag S (S a logic variable) is activated.

- **The steady-state values memorisation:** Once the dynamic steady state detected by the falling of the logic signal S, the values of P_0, Q_0 , V_{t0} and δ_0 are memorized. The difference between the instantaneous values ($\Delta\delta(t)$, $\Delta V_t(t)$) and the memorised values (δ_0, V_{t0}) allows us to calculate the deviations signals $\Delta\delta$ and $\Delta V_t'$.
- **Decoupling control signals calculation:** the coefficients λ and β are computed from the stead state values P_0, Q_0, V_{t0} by using equations eqs. (30) and (31). Fig. 3 shows the block diagram control of the proposed control technique.

control signals are zero in steady state.

Once the decoupling between active and reactive power loop is fulfilled, the active and reactive power are controlled independently. The linear model of active and reactive power loops could be simplified as shown in Fig. 4.

The parameters determining the dynamic behaviour of the active and reactive power loops are the rotational inertia J, the damping coefficient D and the proportional-integral coefficient of the voltage regulator k_p and k_i, respectively.

From Fig. 4.a, the transfer function from reference active power to output active power is expressed by:

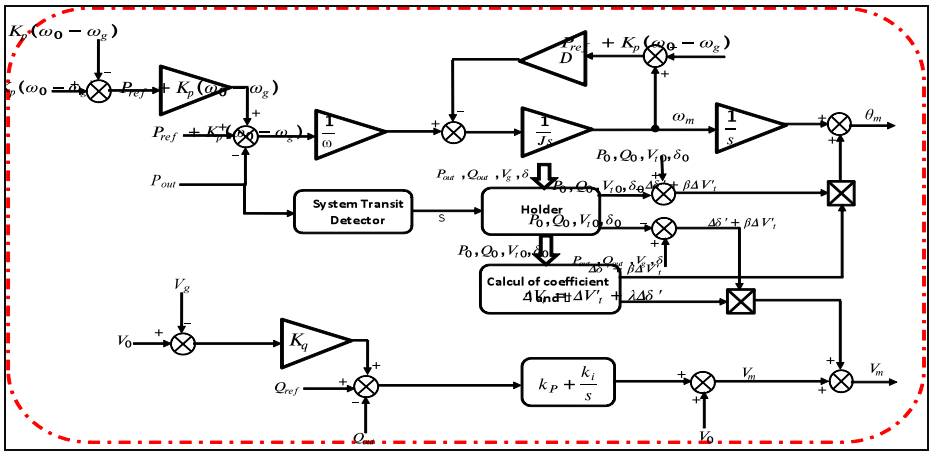

Fig. 3 – Control structure of the proposed VSG.

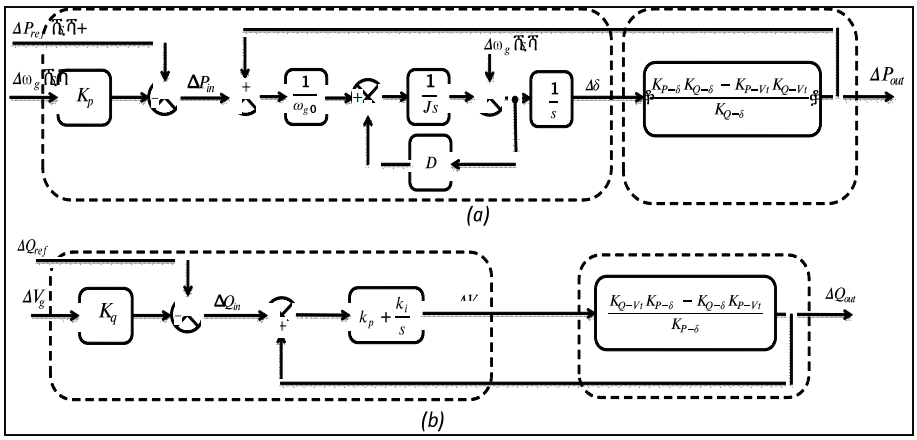

Fig. 4 – Small signal model of the VSG without coupling terms: a) active power loop, (b) reactive power loop.

The system transition, which could be for example variation of active or reactive power reference or connection/disconnection of a local load, is detected by analyzing the active or reactive power evolution. Thus, the active or reactive power is filtered and compared for two successive sampling time; if the difference exceeds certain threshold, the comparison result is one logic meaning that the system is in transit steady state. The output of the transition detector S serves as a trigger input to the holder block; the output of the holder block is changed in the falling of the trigger signal meaning that the steady-state value is updated at the end of system transition. The steady-state values are used to compute the decoupling signal coefficient λ and β based on equations eqs. (30), (31). The control variables deviation $\Delta\theta$ and ΔV could simply calculated as the difference of the steady-state and the instantaneous values.

It should be noted that the proposed control strategy does not change the system static characteristics (active and reactive power droop mechanism) since the decoupling

$$\frac{\Delta P_{out}}{\Delta P_{ref}}(s) = \frac{a_1}{s^2 + a_2 s + a_1}, \tag{32}$$

where

$$a_1 = \frac{D}{J}. \tag{33}$$

$$a_2 = \frac{K_{P-\delta}K_{Q-\delta} - K_{P-Vt}K_{Q-Vt}}{K_{Q-\delta}J\omega_{g0}}. \tag{34}$$

Equation eq. (32) has the same form as the well-known response of a typical 2nd order control system to a step input:

$$G(s) = \frac{\omega_n^2}{s^2 + 2\xi\omega_n s + \omega_n^2}, \tag{35}$$

where ξ is the damping ratio and ω_n is the undamped natural pulsation of the system. The response performance of the system can be changed by changing the damping ratio. Indentifying ω_n and ξ using eq. (32) and eq. (35), we have:

$$\omega_n = \sqrt{\frac{D}{J}}, \tag{36}$$

$$\xi = \sqrt{\frac{1}{JD}} \frac{K_{P-\delta}K_{Q-\delta} - K_{P-Vt}K_{Q-Vt}}{2K_{Q-\delta}J\omega_{g0}}. \quad (37)$$

It can be seen from equations (eqs. 36 and 37) that both the damping ratio ξ and the undamped natural frequency ω_n are affected by D and J. So, the system response speed cannot be adjusted freely without affecting the damping characteristic.

The effect of the control parameters on the dynamic performances and damping ratio of the active power loop are analyzed in detail by [33] and [34]. In this work, the control parameters have been adjusted by trial and error procedure. The rise time and damping factor of the active power loop are chosen as 0.2 s and 0.55 s, respectively; while the proportional-integral coefficients of the reactive power loop are selected to impose a setting time equal to 0.4 s.

The closed loop reactive power transfer function can be derived from Fig. 4.b as follows:

$$\frac{\Delta Q_{out}}{\Delta Q_{ref}}(s) = \frac{bs}{s(1+K_p b)+K_i b}, \quad (38)$$

where

$$b = K_i \frac{K_{Q-Vt}K_{P-\delta} - K_{Q-\delta}K_{Q-Vt}}{K_{P-\delta}}. \quad (39)$$

3. RESULTS AND DISCUSSION

The theoretical analysis presented in previous sections has been verified using Matlab /Simulink environment using the microgrid system presented in Fig 5.

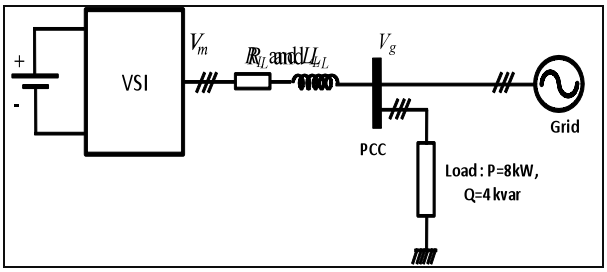

Fig. 5 – The microgrid platform under simulation.

The voltage source inverter (VSI) is connected to the main grid at the PCC through a mixed line impedance. A resistive-inductive load is coupled to the PCC point, this load is supplied by the VSI and the main grid. A conventional and developed VSG approaches are applied on VSI. The key parameters of the steady system are given in Table 1.

Table. 1

Parameters of the microgrid platform.

Parameters	Values
Nominal utility line-line voltage (RMS) (V)	220
Nominal utility frequency (Hz)	50
Dc link voltage (V)	600
Inverter switching frequency (kHz)	4
Inverter output filter inductance (mH)	5
Inverter output filter capacitor (μF)	40
Inverter rated power (kW)	10
Line resistance (Ω)	0.641
Line inductance (mH)	0.32
Virtual inertia (kg.m^2)	0.5
Damping coefficient	10
Active droop coefficient	7957
Reactive droop coefficient	1250

The reactance and resistance R include the distribution line impedance in addition to the impedance of the inter-connecting inductor of the voltage source inverter.

The efficiency of the proposed decoupling VSG control strategy has been compared to the conventional VSG control using different test scenarios as defined below:

- **Test scenario 1: Dynamic performances**
  - case 1: active power analysis
  - case 2: reactive power analysis
- **Test scenario2: Robustness performances**
  - case 1: active power analysis
  - case 2: reactive power analysis

3.1 TEST SCENARIO 1: DYNAMIC PERFORMANCES

In this test scenario we evaluate the dynamic performances of the proposed VSG control to classical one in case of active or reactive variation. Figure 6 shows the pattern test for active power variations; while Fig. 7 shows the pattern test for reactive power variations.

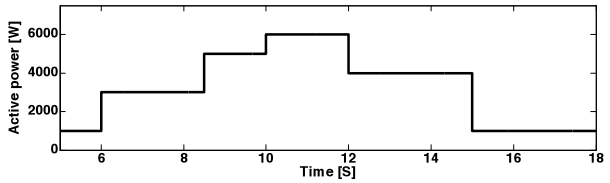

Fig. 6 – Active power variation used in test scenario1.

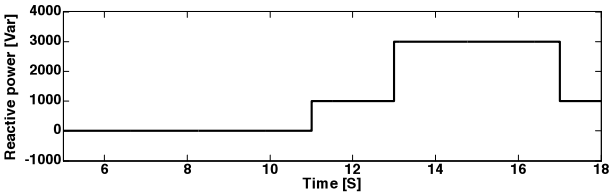

Fig. 7 – Reactive power variation used in test scenario1.

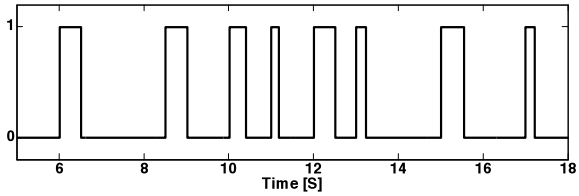

Fig. – 8 Transition signals.

From Fig. 8, the algorithm detects successfully the transition of the active or reactive power. In addition, the decoupling signal parameters are updated in the falling edge of the trigger signal with corresponds to the end of the system dynamic steady state as illustrated in Figs. 9 and 10.

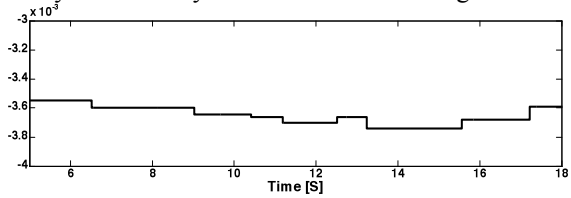

Fig. 9 – Decoupling signal δ.

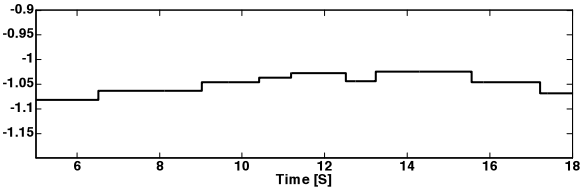

Fig. 10 – Decoupling signal β.

3.1.1 ACTIVE POWER ANALYSIS

Figure 11 shows the corresponding active power using both conventional and proposed VSG control; while Table 2 summarizes the main results of test scenario 1 regarding the active power. From Table 2, it is undeniably clear that the proposed VSG control performs better than the classical one considering the variation of active power. The proposed VSG control reduces the overshoot in case of active or reactive power variations between 71.04 % and 83.76 % for the variations due to active power changes and between 90.66 % and 91.07 % for variations due to reactive power changes. The setting time is between 27.57 % and 49.81 % for the variations due to active power changes and between 90.66 % and 91.07 % for variations due to reactive power changes.

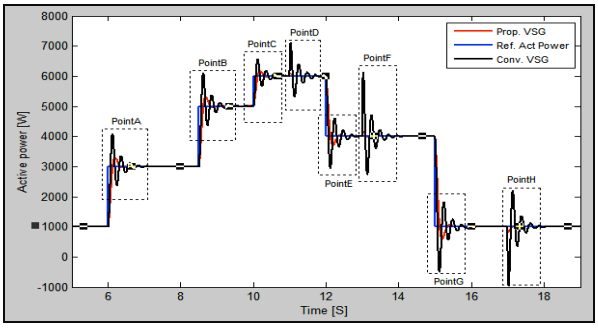

Fig. 11 – Active power variations in case of test scenario 1.

Table 2

Main results of test scenario 1: active power.

Active Power		Overshoot (W)			Setting time (s)		
		Conv. VSG	Prop. VSG	Red. Ratio (%)	Conv. VSG	Prop. VSG	Red. Ratio (%)
Due to active Power variation	A	379	61.55	**83.76**	1.554	0.780	**49.81**
	B	1116	318	71.51	1.330	0.843	36.62
	C	556	161	**71.04**	0.995	0.690	30.65
	E	1059	300	71.67	0.994	0.720	**27.57**
	G	1499	410	72.65	1.410	0.720	48.94
Due to reactive power variation	D	1109	99	**91.07**	0.990	0.440	55.56
	F	2118	195	90.79	1.360	0.632	**53.53**
	H	1949	182	**90.66**	1.420	0.570	**59.86**

3.1.2 REACTIVE POWER ANALYSIS

Figure 12 shows the corresponding reactive power using both conventional and proposed VSG control; while Table 3 summarizes the main results of test scenario 1 regarding the reactive power.

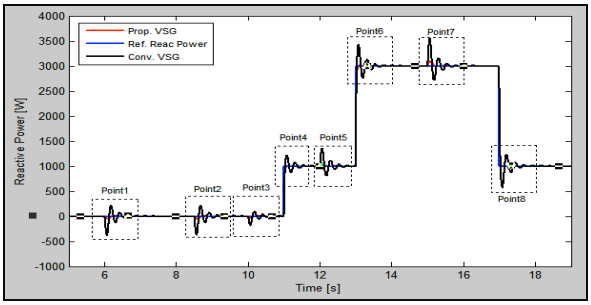

Fig. 12 – Reactive power variations in case of test scenario 1.

From Table 3, we can see clearly that the proposed VSG control outperforms the classical one regarding the variation of reactive power. The proposed VSG control reduces the overshoot in case of active or reactive power variation between 66.60 % and 83.76 % for the variations due to active power changes and between 99.17 % and 99.55 % for variations due to reactive power changes. In the same time, the proposed VSG control reduces the setting time 38.54 % and 52.67 % for the variations due to active power changes and between 60.69 % and 63.64 % for variations due to reactive power changes.

Table. 3

Main results of test scenario 1: reactive power.

Reactive Power		Overshoot (W)			Setting time (s)		
		Conv. VSG	Prop. VSG	Red. (%)	Conv. VSG	Prop. VSG	Red. (%)
Due to an active power variation	1	379.00	61.55	**83.76**	1.554	0.780	49.81
	2	371.10	60.89	83.59	1.431	0.730	48.99
	3	182.30	60.88	**66.60**	0.950	0.530	44.21
	5	361.00	60.00	83.38	0.960	0.590	**38.54**
	7	547.00	90.00	83.55	1.310	0.620	**52.67**
Due to reactive power variation	4	224.00	1.00	**99.55**	0.990	0.360	**63.64**
	6	428.00	3.00	99.30	1.340	0.510	61.94
	8	422.50	3.50	**99.17**	1.450	0.570	**60.69**

3.2 TEST SCENARIO 2: ROBUSTNESS TESTS

In test scenario 1, to compute the decoupling control signals, the line impedance has been supposed to be known with high precision. However. in practical applications the line resistance and inductance drift from real values. To investigate the influence of mismatched line impedance (resistance and inductance variation) on the dynamic performance and decoupling accuracy of the proposed decoupling control scheme, several tests have been carried out as defined below: i) variation of L +/–20 %; ii) variation of R +/–20 %; and iii) variation of R +/–20 % and L +/–20 %. In each case, we analyze the active and reactive power dynamics regarding overshoot and setting time.

3.2.1 ACTIVE POWER ANALYSIS

Table 4 summarizes the results regarding active power variation related to line parameters changes.

Table 4

Active power variations related to line parameters changes. (Conv. VSG: 1372 W; 0.991 s)

Active power		Overshoot		Setting time	
ΔR	**ΔL**	**OS(W)**	**RR (%)**	**ST(s)**	**RR (%)**
0	0	323	76.46	0.469	52.67
0	20	379	72.38	0.637	**35.72**
0	-20	257	81.27	0.637	**35.72**
20	0	265	80.69	0.626	36.83
-20	0	395	**71.21**	0.626	36.83
20	20	319	76.75	0.469	**52.67**
20	-20	203	**85.20**	0.592	40.26
-20	20	454	66.91	0.592	40.26
-20	-20	326	76.24	0.469	**52.67**

3.2.2 REACTIVE POWER ANALYSIS

Table 5 summarizes the results regarding reactive power variation related to line parameters changes.

Table 5

Reactive power variations related to line parameters changes. (Conv. VSG: 466 W; 1.303 s)

Reactive power		Overshoot		Setting time	
ΔR	**ΔL**	**OS(W)**	**RR (%)**	**ST(s)**	**RR (%)**
0	0	11	97.64	0.443	66.00
0	20	48	89.70	0.549	57.87
0	-20	40	91.42	0.549	57.87
20	0	38	91.85	0.552	**57.64**
-20	0	46	90.13	0.552	**57.64**
20	20	12	97.42	0.443	**66.00**
20	-20	81	82.62	0.541	58.48
-20	20	84	**81.97**	0.541	58.48
-20	-20	10	**97.85**	0.443	**66.00**

From Table 5, as for the active power, even the variation of line parameters (R and L) between +20% and –20% the reactive power overshoot using the proposed VSG control is reduced between 81.97 % and 97.85 %; while the reactive power setting time using the proposed VSG control is reduced between 54.67 % and 66.00 %.

3.3 DISCUSSION

Obtained results prove the superiority of dynamic performance of the proposed approach in all considered cases regarding active or reactive power increase or decrease. Thanks to the decoupling between active and reactive power control loops, the stability and tracking performance of the active and reactive power regulation are improved. Thus, a huge improvement in the reduction of the overshoot (between 71.04 % and 91.07 % for the active power and between 66.60 % and 99.55 % for the reactive power). The setting time has been reduced significantly (between 27.57 % and 59.86 % for the active power and between 38.54 % and 63.64 %). In addition, robustness results realized using a line parameters variation between –20 % and +20 % prove definitely the effectiveness of the proposed VSG decoupling control. Even with line parameters variations the overshoot reduction is between 71.20 % and 85.20 % for the active power and between 81.97 % and 97.85 %; while the setting time reduction is between 35.72 % and 52.67 % for the active power and between 57.64 % and 66.00 % for the reactive power. By using the proposed algorithm, it is incontestably apparent that the active and reactive powers react with excellent dynamic as consequence of low interaction between active and reactive powers.

4. **CONCLUSION**

This paper addresses the development of a new VSG control strategy applied to DG unit to improve the stability and dynamic performance of the conventional VSG. the proposed control technique consists in decoupling between the active and reactive powers loops based on small signal analysis of active and reactive powers expressions leading to the separation of the active and reactive power loops. The proposed VSG control has been implemented and compared to the basic VSG scheme using Matlab/Simulink environment. Simulation results show a significant improvement in term of the overshoot and setting time reduction. Moreover, robustness tests realized using a line parameters deviation confirm the effectiveness of the proposed VSG decoupling control. The coupling effect between active and reactive power is almost eliminated without influencing the inertia support feature of VSG control. Therefore, the oscillations and overshoots of active and reactive power are considerably reduced, and the system stability recovered.

Received on July 23, 2019

REFERENCES

1. T. Zebbadji, R. Ibtiouen, S. Hadji, *Power Flow Analysis and Cross-Current Optimisation for Parallel Connected Inverters* Rev. Roum. Sci. Techn. Électrotechn. et Énerg. **64**, *3*, pp. 137–142 (2019).
2. T. L. Vandoorn, B. Meersman, L. Degroote, B. Renders, L. Vandevelde, *A control strategy for islanded microgrids with dc-link voltage control*. IEEE Trans. Power Del. **26**, pp. 703–713 (2011).
3. J. Liu, Y. Miura, T. Ise, *Comparison of dynamic characteristics between virtual synchronous generator and droop control in inverter-based distributed generators*. IEEE T Power Electr., **31**, pp. 3600–3611 (2016).
4. Q.-C. Zhong, *Virtual Synchronous Machines: A unified interface for grid integration*. IEEE Power Electron. Mag., **3**. pp. 18–27 (2016).
5. Y. Zhu, F. Zhuo, F. Wang, B. Liu, R. Gou, Y. Zhao, *A virtual impedance optimization method for reactive power sharing in networked microgrid*. IEEE T Power Electr., **31**, pp. 2890–2904 (2016).
6. Z. Wang, H. Yi, J. Wu, F. Zhuo, F. Wang, Z. Zeng, *Dynamic performance analysis of paralleled virtual synchronous generators under grid connected and islanded mode*, in Proc IEEE. Applied Power Electronics Conference and Exposition (APEC), pp. 1326–1332, 2017
7. P. Monica, M. Kowsalya, *Control strategies of parallel operated inverters in renewable energy application: A review*. Renewable and Sustainable Energy Reviews, **65**, pp. 885 – 901 (2016).
8. Z. Shuai, Y. Hu, Y. Peng, C. Tu, Z.J. Shen, *Dynamic stability analysis of synchronverter-dominated microgrid based on bifurcation theory*, IEEE Transactions on Industrial Electronics, **64**, *9*, pp. 7467–7477 (2017).
9. Z. Shuai, W. Huang, C. Shen, J. Ge, Z.J. Shen, *Characteristics and restraining method of fast transient inrush fault currents in synchronverters,* IEEE Trans on Industrial Electronics, **64**, *9*, pp. 7487–7497 (2017).
10. Q.C. Zhong, G. Weiss, *Synchronverters: inverters that mimic synchronous generators*, IEEE Trans. On Ind. Electron., **58**, pp. 1259–1267 (2011).
11. J.M. Guerrero, L.G. de Vicuña, J. Matas, M. Castilla, J. Miret, *Output impedance design of parallel-connected UPS inverters with wireless load-sharing control*, IEEE Trans. Ind. Electron., **52**, pp. 1126–1135, Augst 2005.
12. J.M. Guerrero, L. Hang, J. Uceda, *Control of distributed uninterruptible power supply systems*, IEEE Trans. Ind. Electron., **55**. pp. 2845–2859 (2008).
13. Q.C. Zhong. G.C. Konstantopoulos. B. Ren, M. Krstic. *Improved synchronverters with bounded frequency and voltage for smart grid integration*. IEEE Trans. Smart Grid. published online in 2016.
14. H-P. Beck, R. Hesse, *Virtual synchronous machine*, in Proc. 9th Int. Conf. Elect. Power Quality Util., pp. 1–6, 2007.
15. T. Wu. Z. Liu. J.J. Liu, S. Wang, Z.Y. You, *A unified virtual power decoupling method for droop-controlled parallel inverters in microgrids*, IEEE Trans. Power Electron., **31**, *8*, pp. 5587–5603 (2016).
16. B. Li, L. Zhou, X. Yu, C. Zheng, J. Liu, *Improved power decoupling control strategy based on virtual synchronous generator*, IET Power Electronics, **10**, pp. 462–470 (2017).
17. L. Bin, Z. Lin, Y. Xirui, Z. Chen, L. Jinhong, X. Bao, *New control scheme of power decoupling based on virtual synchronous generator*, Proc. IEEE Power and Energy Conference at Illinois (PECI), pp. 1–8, 2016.
18. M. Li, Y. Wang, N. Xu, et al., *A power decoupling control strategy for droop-controlled inverters and virtual synchronous generators*, Power Electronics and Motion Control Conference, IEEE, pp. 1713–1719, 2016.
19. Z.Y. Zhuo, F. Wang *et al.*, *A wireless load sharing strategy for islanded microgrid based on feeder current sensing*. IEEE Trans. Power Electron. **30**, *12*, pp. 6706–6719 (2015).
20. M.H. Michaelson, D.J. Jiang, *Accurate reactive power sharing in an islanded microgrid using adaptive virtual impedances*, IEEE Trans. Power Electron. **30**, *3*, pp. 1605–1617 (2015).
21. H.J. Li, Y.W. Blaabjerg, *An enhanced islanding microgrid reactive power. imbalance power. and harmonic power sharing scheme*, IEEE Trans. Power Electron, **30**, *6*, pp. 3389–3401 (2015).
22. Z.P. Zhao, H. Cai, et al., *Power decoupling strategy based on 'virtual negative resistor' for inverters in low voltage microgrids*, IET Power Electron., **9**, *5*, pp. 1037–1044 (2016).
23. K. Debrabandere et al., *A voltage and frequency droop control method for parallel inverters*. IEEE Trans. Power Electron., **22**, *4*. pp. 1107–1115. 2007.
24. C.T. Lee, C.C. Chuang, C.C. Chu, *Control strategies for distributed energy resources interface converters in the low voltage microgrid*, in Proc. IEEE Energy Convers. Congr. Expo. San Jose. CA. USA, pp. 2022–2029, 2009.
25. Z. Peng, J. Wang. D. Bi, Y. Dai, Y. Wen, *The Application of Microgrids Based on Droop Control with Coup*ling *Compensation and Inertia*, IEEE Trans. Sustain. Energy., **PP**, *99*, pp. 1–6, 2017.
26. H. Han, X.C. Hou, J. Yang, J. Wu, M. Su, J.M. Guerrero, *Review of power sharing control strategies for islanding operation of AC microgrids*, IEEE Trans. Smart Grid, **7**, *1*. pp. 200–215 (2016).
27. M.B. Delghavi, A. Yazdani, *An adaptive feedforward compensation for stability enhancement in droop-controlled inverter-based microgrids*, IEEE Trans. Power Del., **26**. *3*, pp. 1769–1773 (2011).
28. A.H. Amirnaser Y.J. Gẻza. B. Benoit, *A gain-scheduled decoupling control strategy for enhanced transient performance and stability of an islanded active distribution network*, IEEE Trans Power Deliv. **29**, pp. 560–569 (2014).
29. M.A. Azzouz, E.F. El-Saadany, *Multivariable DG impedance modeling and reshaping for impedance stabilization of active distribution networks*, IEEE Transactions on Smart Grid, **9**, *3*, pp. 2166 – 2179 (2018).
30. H. Yibin, Y. Xiangwu. L. Dongxue. L.Xinxin, Z. Bo, *Experimental study of micro sources inverter based on virtual synchronous generator*, in Proc. IEEE Conf. Electrical and Electronic Engineering, pp.2433–2438, 2017.
31. J. Meng, X. Shi, Y. Wang, C. Fu, *A virtual synchronous generator control strategy for distributed generation*, in Proc. IEEE China Int. Conf. Electricity Distribution, pp. 495–498, 2014.
32. S. D'Arco, J.A. Suul, O.B. Fosso, *Small-signal modeling and parametric sensitivity of a virtual synchronous machine in islanded operation*, Int. Journ. Electrical Power & Energy Systems, **72**, pp. 3–15 (2015).
33. S. Dong, Y.C. Chen, *Adjusting Synchronverter dynamic response speed via damping correction loop*, IEEE T Energy Conver, **32**. pp. 608–619 (2017).
34. F. Wang, L. Zhang, X. Feng., H. Guo, *An Adaptive Control Strategy for Virtual Synchronous Generator*. IEEE Trans. On Ind. Electron., **54**. pp. 5124–5133 (2018).
35. L. Sasthankutty, R. Ramabadran, *Stability Evaluation of Four Phase High Gain Converter by Small Signal Modeling*, Rev. Roum. Sci. Techn. Électrotechn. et Énerg., **65**, *1–2*, pp. 75–80 (2020).